PAHs and fullerenes as structural and compositional motifs tracing and distinguishing organic carbon from soot

B. Apicella [a,*], C. Russo [a], A. Carpentieri [b], A. Tregrossi [a], A. Ciajolo [a]

[a] Istituto di Scienze e Tecnologie per l'Energia e la Mobilità Sostenibili (STEMS)– CNR – P.le V. Tecchio, 80 – 80125 Napoli, Italy
[b] Dipartimento di Scienze Chimiche, Università "Federico II", Via Cintia – 80125 Napoli, Italy

ARTICLE INFO

ABSTRACT

Examining the features distinguishing organic carbon from soot is crucial for understanding the source, the effect on the environment and their respective role in aerosol chemistry and soot formation. Beside to the obvious PAH picking-out in the low-mass mode (C number < 40), the challenging identification of PAHs in the high-mass mode (C number > 40) of organic carbon, separated by carbon particulate matter extraction from young and mature soot thermophoretically sampled in premixed flames, was done by laser-desorption-time-of-flight mass spectrometry, exploiting the laser power increase. The perusal of organic carbon mass spectra through mathematical tools in comparison to aromatic and alkyl-substituted PAH-laden samples and the persistence of high-mass mode at high laser power led to exclude the contribution of dimers and alkyl-bridged PAHs attributing the second mode to both fully-benzenoid and cyclopenta-PAHs.

Profound differences between mass spectra of organic carbon and soot were noticed as neither molecules nor radicals of PAHs could be drawn out from soot, even at high laser power, and only small radicals and carbon clusters like fullerenes were observed, especially for young soot. These inferences evidenced the importance of analysing separately organic carbon and soot especially if insights into soot particles nucleation are to be obtained. In the case of benzene flame, already at the inception, soot consists of strongly tangled aromatic motifs crosslinked each other, presumably deriving from reactive coagulation/clustering of relatively small aromatic hydrocarbons/radicals early formed. In methane and ethylene flames, coalesced liquid-like material composed of soot and PAHs is formed and transformed later on undergoing some carbonization and molecular growth, respectively.

1. Introduction

Carbon particulate matter (PM), emitted from combustion-based systems and present in polluting environmental aerosols, is largely composed of solid carbon particles, often named interchangeably as black carbon, soot, elemental carbon and refractory carbon, mixed (externally or internally) in variable proportions with many organic species, the latter ones grouped under categories of different name as organic carbon, soluble organic fraction, not-refractory organic carbon, condensed species. The different composition and properties of carbon PM (e.g. hydrogen/carbon (H/C) ratio, solubility/insolubility, light absorption) in dependence on the emitting source are very important since affecting both human health, as related to PM inhalability and cancerogenic effects [1], and the climate change, due to PM interactions with solar radiation and water vapour, cloud formation and

precipitation [2,3].

Mass spectrometry (MS) is a diagnostic tool able to separate species in a wide molecular weight range, making this technique among the diagnostics more suitable to face an intricate problem as the characterization of carbon PM in the main components [4–12]. MS has been specifically developed for the detection of organic pollutants in a molecular mass range enough wide to include polycyclic aromatic hydrocarbons (PAHs) and the first smaller soot particles [[13,14] and references therein]. Pioneering works of MS have been carried out to analyse soot and surrounding hydrocarbons by Homann and Wagner in the 1960s-1970s [4], as further reviewed in [5]. Later on, in the 1980s-1990s, MS has been used for shedding light on soot precursors and the chemical transformations occurring during the evolution from a liquid-like phase to mature soot [5–7]. It has been found that such transformations are associated to some specific changes of soot

characteristics like H/C, light absorption [8–11] and reactivity [12]. Importantly, in addition to PAHs, particular carbon molecules as fullerenes have been found in flames in form of ions by MS [15] and as neutral species by extraction and analysis of benzene flame soot [6]. Real-time aerosol MS analysis (RTAMS) has been applied for discriminating PAH-containing particles from soot aggregates in flames of acetylene [16], whereas a multi-technique approach encompassing two-step laser MS (L2MS), secondary ion MS (SIMS), has been developed for characterizing the particulate and gas-phase compositions of combustion by-products [17,18]. Soft removal of molecules adsorbed on the particle surface has been utilized to reduce both their fragmentation and the in-depth damaging of the underlying carbon matrix [19,20]. A reflectron time-of-flight mass spectrometer has been applied on-line to a premixed flame for exploring soot particle composition as it develops in flames, through particles laser ablation and ionization [21]. The laser ablation approach has been used to provide a complete mass spectrum of carbon PM, including both semivolatile and refractory components, in different flame conditions [22]. Recently, soot particle aerosol mass spectrometry (SP-AMS) has been applied for distinguishing refractory carbon from the refractory and non-refractory organic carbon in the carbon particles produced by a miniCAST soot generator [23]. Interestingly, MS has been implemented also in astrophysical field, for proofing the interaction processes of interstellar dust with high-energy projectiles yielding large molecular compounds observed in space [24,25].

The importance of distinguishing soot from organic carbon is well recognized in aerosol chemistry as well as in soot formation research fields since the discrimination between organic carbon and soot is crucial for understanding their origin and the possible interconnections between soot and organic carbon formation and transformation [11,20].

The interference of PAHs on the determination of soot properties has been observed in early work where the H/C atomic ratio of carbon particles measured by MS under lower vacuum conditions, resulted to be considerably high (H/C > 0.5), i.e. next to the H/C ratio typical of organic species extracted by dichloromethane [26], due to the condensation and/or adsorption of PAHs of sufficiently low vapor pressure [4]. Actually, MS and gaschromatography coupled to MS (GC–MS) of flame gases have shown the occurrence of gas-phase PAHs [17,27], which can condense on soot especially in the sampling line (probe walls, filter) so biasing the determination of soot composition and properties. Likewise, also other spectroscopic and microscopic diagnostics based on scanning tunnelling microscopy (STM) [28] and light absorption [29] have shown to be mostly sensitive to PAHs as main components of organic carbon mixed with soot.

The reciprocal interference is particularly relevant for what regards the study of soot particle nucleation. For instance, MS analysis carried out on the whole carbon PM [e.g. 7, 30, 31] can be deceptive since dominated by the PAH contribution, even more if carried out on the PAHs deposited/condensed on the grid upon heating of the whole carbon PM [32]. In fact, already at particle inception the solid carbon component appears quite physically and chemically different in comparison to PAHs. Differently from them, soot is insoluble and poor in hydrogen, absorbing in the visible, not fluorescing [4,9] and producing laser induced incandescence signals and peculiar XRD and Raman spectra. The unique commonality between PAHs and soot consists in the close resemblance of fringes identified by TEM in the soot nanostructure with polyaromatic ring structures [28]. Definitely, the analysis of whole carbon PM provides data that can be misleading because of the reciprocal organic carbon and soot interference. Indeed, soot component interference occurring toward large masses, hinders the detailed investigation of PAH component growth, whereas organic carbon can hinder the low-medium molecular mass range investigation of soot, overwhelmed by PAHs condensed on soot particles.

With the aim of detailing the composition of organic carbon assessing its different features in respect to soot, in this work laser desorption time of flight mass spectrometry (LDI-TOFMS) has been applied to organic

carbon and soot components of carbon PM thermophoretically deposited from premixed flames of methane, ethylene and benzene featured by different relative amounts of organic carbon and soot. Notably, prior work at low/medium laser power conditions has shown that PAHs constituting organic carbon could be easily detailed, whereas the ineffectiveness of LDI-TOFMS to get significant signals from soot leads us to resort to the laser power increase (90% of maximum). The main part of the work is focused on the LDI-TOFMS analysis at low laser power of organic carbon extracted from carbon PM samples at the beginning and the end of soot formation region, to give details on its composition as soot formation progresses. The perusal of LDI-TOFMS spectra of organic carbon has been supported by the application of Fast Fourier Transform (FFT) method and the evaluation of the double bond equivalence (DBE) number. Additionally, the LDI-TOF mass spectra of organic carbon have been compared to those of PAH-laden samples (asphaltenes and pitches derived from coal and petroleum), analysed in the same instrumental conditions, to recognize signatures of specific PAH classes (unsubstituted, aliphatic–substituted PAHs and dimers) present in the organic carbon.

Exploratory work on LDI-TOFMS spectra of soot is reported in the last part of the paper to infer its different features in comparison with those of organic carbon also analysed at high laser power. The tendency of soot particles to fragment and to form carbon clusters in high laser power conditions, previously found off-line by Laser Microprobe-MS [7] and LDI-MS [7,33,34], and on-line by molecular-beam TOF-MS [35], RTAMS [16] and SP-MS [23], has been exploited for the analysis of the main differences in young and mature organic carbon and soot components.

2. Experimental

2.1. Organic carbon, soot and PAH-laden samples

Carbon PM was thermophoretically sampled in premixed sooting flames of methane, ethylene and benzene produced at atmospheric pressure on a commercial McKenna burner at the same cold gas velocity of 4 cm/s and different equivalence ratio, Φ (Φ = 2.40 for methane flame, Φ = 3.03 for ethylene flame and Φ = 2.00 for benzene flame). Carbon PM were sampled at the opposite extremes of the soot formation flame region located between 6 and 14 mm height above the burner (HAB) in all flames, as briefly described in the Supplementary Material, where more details on the experimental conditions are reported. Specifically, soot formation starts at low flame position, around 6–7 mm and ends at high flame position, around 14 mm HAB, where soot formation attains the maximum concentration (Supplementary Material).

Thermophoretic sampling was carried out by fast insertion of a glass plate 75 × 25 × 1 mm) rotating by a gear motor with a frequency of 1.4 Hz and setting the total deposition time for each sample at 25 s [36]. Each lap lasts 700 ms: the plate remains in flame just 60 ms, during the remaining time the plate and the deposited material are at room temperature, allowing for a cooling time of 640 ms after each insertion.

It is noteworthy that the thermophoretic sampling was preferred to the probe sampling to avoid the interference of gas-phase PAHs, which in the latter case condense in the sampling line and completely dominate the mass spectrum of the organic carbon [36].This can be observed in Fig. S1 of supplemental material, where the LDI-TOFMS spectra of mature organic carbon (ethylene flame) sampled by probe and by thermophoretic deposition are contrasted. Carbon PM samples were scratched from the plate and extracted with dichloromethane (DCM) for separating organic species from solid carbon particles insoluble in DCM, referred to as soot. The organic species soluble in DCM are mostly constituted of organic compounds volatilizing at temperature ≤ 450 °C (70–80 wt%) [37,38], so they are hereafter named as organic carbon corresponding to what is also termed as non-refractory organic carbon in aerosol science and atmospheric chemistry [22,23,37,39].

Organic carbon, labelled as young and mature referring to the PM

sampled at the beginning and the end of the soot formation region, respectively, was analysed in comparison to mixtures of standard PAHs, asphaltenes and two pitch samples, altogether classified as PAH-laden samples. The two pitches are an aliphatic pitch, with high aliphatic carbon content, and an aromatic pitch, with high aromatic carbon content. The source specification of young and mature organic carbon and soot samples along with those of PAH-laden samples are gathered in Table 1.

2.2. Laser desorption ionization-time of flight mass spectrometry (LDI-TOFMS)

LDI-TOFMS spectra were recorded on positive reflectron mode on a SCIEX TOF/TOF™ 5800 System using a N_2-laser at 40 and 90% of the maximum nominal power per unit area ($\sim 10^5$ W/cm^2, which corresponds to a fluence ~ 1 mJ/cm^2). The target was prepared by depositing on a standard stainless steel plate the sample dissolved/dispersed in a suitable solvent (DCM, toluene, or N-methylpyrrolidinone (NMP)). Only carbon samples dispersed in NMP were heated, after deposition on the plate, at about 100 °C for few minutes for evaporating the solvent. It is worth to note that the use of matrices can be avoided as carbon samples are able to absorb the laser beam ($\lambda = 337$ nm) acting as a self-matrix matrix [40–42]. Each spectrum represents the sum of 12,000 laser pulses from randomly chosen spots per sample position.

Fast Fourier Transform (FFT) analysis was applied to both organic carbon and soot to compute the discrete Fourier transform (DFT) of repetitive signals like those featuring mass spectra of flame-generated organics as PAHs and carbon clusters. A graphic software (Origin) was used for data analysis. More details on the method as applied to mass spectra are reported in Przybilla et al. [43].

The DBE number, also called degree of unsaturation, was calculated for organic carbon from the structure of the chemicals considering that each π bond or ring generates one DBE. If the compound contains the elements C, H, O, and N, the DBE for the general formula $C_xH_yN_zO_n$ is calculated as follows [44]:

$$DBE = x - y/2 + z/2 + 1.$$

In this work the DBE was determined for each mass peak considering the simplified formula for C_xH_y hydrocarbons: DBE = x-(y/2) + 1 by an home-made software [45]. Iso-abundance graphs were drawn in the Origin software by plotting the DBE number and the relative intensity against the carbon number (CN).

Table 1
List of flame-generated organic carbon, soot and PAH-laden samples with source specification.

Flame-generated organic carbon and soot samples	Source
Methane young organic carbon and soot	Methane flame (HAB = 7 mm)
Methane mature organic carbon and soot	Methane flame (HAB = 14 mm)
Ethylene young organic carbon and soot	Ethylene flame (HAB = 6 mm)
Ethylene mature organic carbon and soot	Ethylene flame (HAB = 14 mm)
Benzene young organic carbon and soot	Benzene flame (HAB = 7 mm)
Benzene mature organic carbon and soot	Benzene flame (HAB = 14 mm)
PAH-laden samples	
Mixture of 5 fully-benzenoid PAHs (pyrene, dibenzo(a,h) anthracene, benzo(b)crisene, benzo (g,h,i)perylene, coronene) and 4 cyclopenta-PAHs at the same concentration	Sigma-Aldrich
Asphaltenes (heptane-insoluble #6 commercial heavy oil)	ASTM D3279
Aromatic pitch	Electrode binder pitch (Rutgers): 65996-93-2
Aliphatic pitch	Petroleum pitch (Rutgers): 68187-58-6

3. Results and discussion

3.1. Overall assessment

The paper reports LDI-TOFMS analysis of organic carbon and soot that have been selected on the basis of some outcomes relative to their response to the LDI-TOFMS observed in prior work. The preliminary work has regarded the LDI-TOFMS analysis of all samples (young and mature organic carbon and soot) deposited, respectively, just after soot inception and at the end of soot formation region of methane, ethylene and benzene premixed flames as described in the Supplementary Material and references therein. It is worth to underline that organic carbon, definitely prevailing on soot at the beginning of the investigated methane and ethylene flames, persists throughout the soot formation region, particularly in the methane flame where the organic carbon/soot mass ratio is much higher (around 1, at the end of the flame) in respect to that of ethylene flame (around 0.6, at the end of the flame). By contrast, organic carbon in the benzene flame is early formed and completely consumed, because of the partial overlapping of oxidation and pyrolytic regions in the atmospheric pressure conditions, so that too few amounts of organic carbon, mainly constituted of phenols [6], hindered the LDI-TOFMS analysis for the organic carbon derived from the benzene flame. Because of this, only the LDI-TOFMS of organic carbon sampled in the ethylene and methane flames could be analysed. After an overall description of the mass spectral behaviour of methane and ethylene organic carbon samples (Figs. 1 and 2), the perusal of the LDI-TOFMS analysis has been mainly devoted to the ethylene organic carbon samples.

Organic carbon samples have been analysed at low/medium laser power conditions of the LDI-TOFMS instrument (40% of the maximum nominal power), corresponding to the MS conditions generally used for routinely analysing organic samples like polymers and biological samples [46]. These conditions limit fragmentation [33], as verified on PAH standard mixtures and PAH-laden samples. On the other hand, the low/medium laser power conditions resulted almost completely ineffective for soot analysis, as typically found for soot aggregates requiring higher levels of irradiance [7]. Consequently, high laser power (90% of the maximum power) has been used for analysing the features of soot in comparison to those of organic carbon analysed in the same high laser power conditions. Fortunately, just the severity of laser conditions
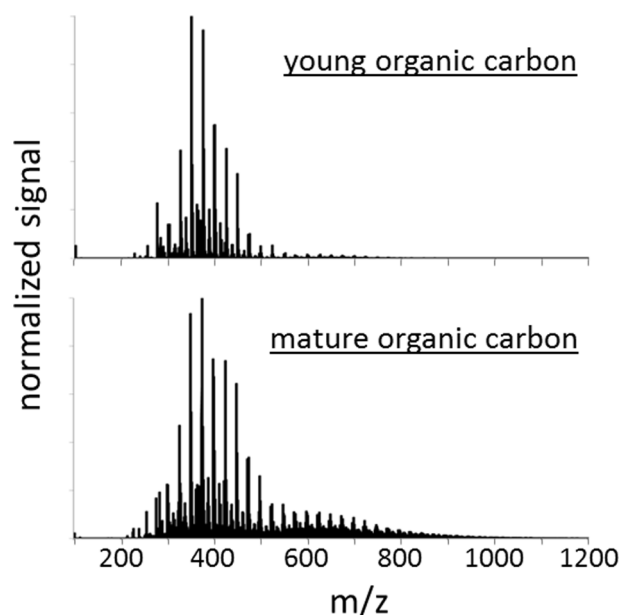

Fig. 1. Mass spectra of ethylene young (up) and mature (down) organic carbon at low laser power.
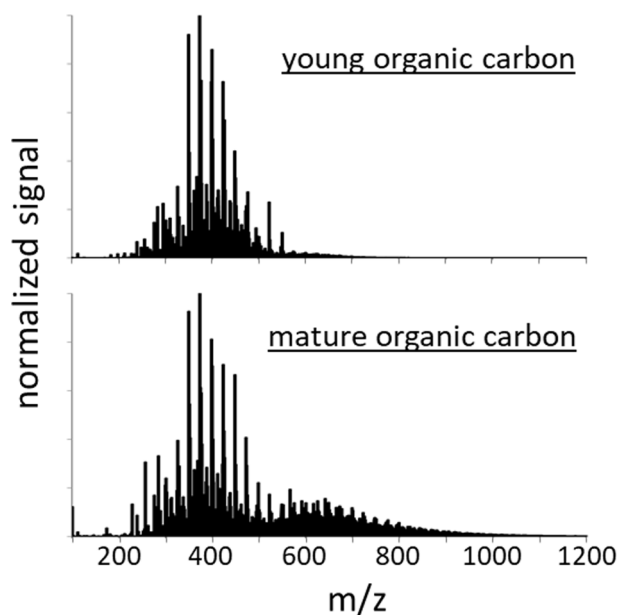
Fig. 2. Mass spectra of methane young (up) and mature (down) organic carbon at low laser power.

resulted to be further informative about organic carbon composition through the analysis of its behaviour under stressing high laser power conditions in comparison with that found for PAH-laden samples and soot.

3.2. Organic carbon

3.2.1. Organic carbon composition: Mass spectra at low laser power

The mass spectra of young and mature organic carbon for the ethylene and methane flames are reported in Fig. 1 and Fig. 2, respectively, in a wide mass range to show an overview of mass spectral similarities and differences. Due to the selective effect of thermophoretic sampling toward large PAHs (C ≥ 22–24) [36], almost all volatile and semivolatile PAHs, $m/z < 200$–250, mostly present in gas phase [17,18], are lacking in young and mature organic carbon samples (Figs. 1 and 2). The predominant mass distribution in the m/z 200–500 range is observed in all mass spectra of young and mature organic carbon (Figs. 1 and 2), exhibiting the maximum around m/z 350–374 and a sharp decrease up to m/z 500. Above m/z 500 a smooth rise-decay profile of the signal intensity can be observed, peaked around m/z 620 and ending at about m/z 1000. This second mode of molecular mass distribution, just outlined for young organic carbon, appears much more relevant for the mature organic carbon (lower part of Fig. 1), suggesting the slight occurrence of molecular growth as soot ages.

Two sequences of different intensity due to even- (the major peak sequence) and odd-C-numbered PAHs (the minor peak sequence) [18] spaced by a mass difference of 24 units, are evident, especially in the first low mass mode of both young and mature organic carbon (see zoom of spectra in Supplementary Material, Fig. S2). This peculiar trend is traceable back to the 24/26 rule assessed for mass spectra of organic samples coming from high temperature processing [42,47], where the PAH formation is attributed to PAH growth by C_2 and/or C_2H_2 units. This is a typical trend of PAH distribution previously observed up to 300–400 mass units by gaschromatography-MS, liquid chromatography-MS and direct injection into MS of organic carbon derived from flame soot [7,48].

It is also worth to note that the parent peak (M$^+$) is predominant in comparison to (M−1)$^+$ peak in the major peak sequence of the even-carbon numbered PAHs, while the minor peak sequence exhibits a similar intensity of (M−1)$^+$ and M$^+$ mass peaks, attributed to the easy

loss of hydrogen linked on methylene bridge typical of odd-C-numbered PAHs as cyclopenta-substituted PAHs [48].

The similarity of the mass spectra of young and mature organic carbon probed from aliphatic fuels (ethylene and methane) in spite of the different flame conditions (Figs. 1 and 2) is noteworthy. With regard to the flame position, a more evident bimodality in the mass spectrum can be noticed for mature organic carbon, confirming the enrichment in heavier species along the soot formation region, regardless of the hydrocarbon fuel used.

More chemical detail on the evolution of the organic carbon in the soot formation region is given by the H-C plot reporting the hydrogen number versus the carbon number, where each point corresponds to one C_xH_y molecule [15,49,50]. The H-C plots of young and mature ethylene organic carbon displayed in Fig. 3 put well in evidence what is visualized in Figs. 1 and 2: i) the predominance of individual PAH molecules enclosed in a relatively small carbon number range (CN 20–40), ii) the enrichment in heavier PAH species along the soot formation region [7,49] and iii) the predominance of even-C-numbered (with even hydrogen number) (darker points) up to the trough noticed between low and high mass species at about m/z 500, corresponding in Fig. 3 to CN = 40. Above this boundary, it can be noticed that even- and odd-C-numbered species, with even and odd number of hydrogens, concur with a similar intensity to large mass PAHs (CN > 40), demonstrating that both PAH molecules and π-radicals contribute to large masses [51].

The appearance of a trough in the mass distribution around m/z 500 and the relative enrichment in odd-C numbered PAHs as molecular mass rises [51,52] could be due to a structural modification. It has been suggested that the change in the spatial arrangement from planar two-dimensional (2D) (fully benzenoid) PAHs toward to curved and/or concave PAH-containing systems, based on cyclopenta-substituted PAHs [51], approximating to compact closed-shell 3D young soot particles [42] could be at the basis of this mass spectral feature. The rearrangement of a PAH with an externally-fused cyclopenta group toward a curved PAH having an internally-fused cyclopenta group is a process (Stone-Wales pyracyclene rearrangement [53]) observed under conditions pertinent to combustion [54,55]. Just the larger contribution at high masses of odd-C-numbered species typical of cyclopenta-PAHs could support this interpretation.

It is interesting to note that bulk chemical and spectroscopic diagnostics do not catch the heavier-PAH enrichment during soot formation, i.e. the increase of the second mode. As matter of fact, only a little variable absorption coefficient and an almost constant H/C atomic ratio (around 0.5) of organic carbon have been found along the soot formation region of premixed flames [30]. The bimodality of the LDI-TOF mass spectra, (Figs. 1 and 2) is instead consistent with that observed in the molecular mass distribution evaluated by both size exclusion chromatography [42] and on-line molecular beam MS measurements of organic carbon in premixed flames burning at low [51] and atmospheric pressure [52], demonstrating that species in the higher molecular mass range are not artifacts of LDI-TOFMS conditions.

Importantly, the H-C plot shows that all the molecular formulas of species identified are enclosed in a band delimited by a black and red line connecting the molecular formulas of highly-condensed PAH systems of six-membered rings (pericondensed) (black line) and linearly anellated (catacondensed) (red line), respectively. PAHs with the same number of C atoms, but different numbers of H atoms i.e. from the same mass spectrometric groups (in vertical on Fig. 3), present very different structures and mechanisms of formation [15]. The band widening towards larger species indicates the increase of more hydrogenated PAHs (H-rich PAHs) with the carbon number increase. Many possible H-rich PAH structures can be responsible as those coming from partial hydrogenation and alkyl substitution of PAH, dimerization and biaryl species formation. Eventually, pericondensed PAH molecules/radicals, already prevalent in the low mass region, having more elongated carbon backbones featured by bays and coves, are possible H-rich candidates [51].
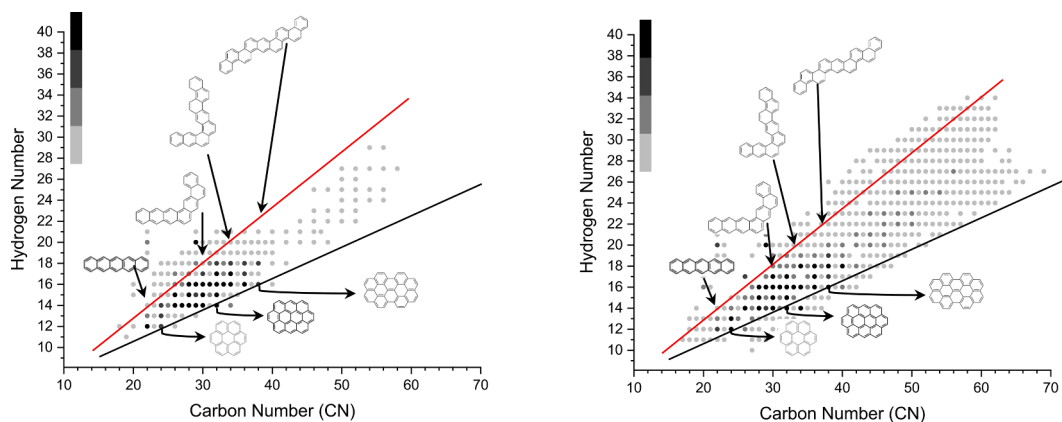
Fig. 3. H-C plot of the molecular formulas [Hydrogen Number (y) vs. Carbon Number (x) in C_xH_y masses] in young (left) and mature (right) ethylene organic carbon. The *peri*-condensed and cata-condensed PAH limits are reported as black and red lines, respectively. Molecular structures of the most intense peaks along the lines assigned to PAHs are also reported. (For interpretation of the references to color in this figure legend, the reader is referred to the web version of this article.)

The role of PAH dimerization in soot formation is currently object of many studies [e.g. [56] and references therein] and in our study the attribution of the second mode to the clustering of PAHs by dimerization would seem supported by the fact that the molecular masses, m/z 500–1000, featuring this mode, are approximately twice the molecular mass of more abundant lighter PAH (m/z 200–500). Furthermore, the crowding of mass spectra exhibiting peaks at every mass unit above m/z 500 (Fig. 3), could be attributed to oligomeric species termed aromers by Homann, which has attributed a forest of peaks observed in mass spectra of flame ions by TOFMS to species "encompassing two agglomerated PAHs to the nearly closed as well as H-containing cages" [15,57].

The occurrence of PAH dimers and their role as soot precursors alternative to individual PAHs have been early suggested [58,59]. Physical dimerization between PAHs such as pyrene has been initially indicated to be involved in soot inception [60], however, it has been argued that the high temperature does not favour physical dimerization [61,62]. In alternative, reactive coagulation leading to large PAHs, suggested in early work [49], has been recently reconsidered by Eaves [63] and Kholghy [64,65] as involving covalent carbon–carbon bonds between PAHs with the formation of both homogeneous and heterogeneous dimers [64]. This mechanism has been added to that involving the reversibility of dimerization process with the formation of PAH clusters linked by Van der Waals forces [65]. Interestingly enough, beside physically- and chemically-linked PAHs, another kind of PAH dimers connected by aliphatic bridges has been recently detected by tandem MS-MS [66]. To ascertain the nature of species constituting organic carbon with particular regard to those featuring the second mode of the molecular distribution, the effect of laser power increase has been here studied and below reported.

3.2.2. Organic carbon composition: Mass spectra at high laser power

The mass spectrum of ethylene mature organic carbon measured at high laser power is contrasted with that measured at low power in Fig. 4. Overall, it can be seen that the high laser power spectrum in the whole MS range becomes crowded of peaks next to the PAH parent peaks, and the even- and odd-C-numbered PAH sequences become more similar in intensity, especially above m/z 500. Moreover, the maximum of the first dominant distribution mode appears just slightly downshifted, whereas the position of the second mode is almost unchanged in comparison with the mass spectrum measured at low laser power (upper part of Fig. 4). Summing up, a relative stability of the organic carbon components is demonstrated by the fact that the high laser power, even causing some PAH dehydrogenation and radical formation, does not affect and mainly preserves the original distribution of PAHs, at least up to about m/z 500.

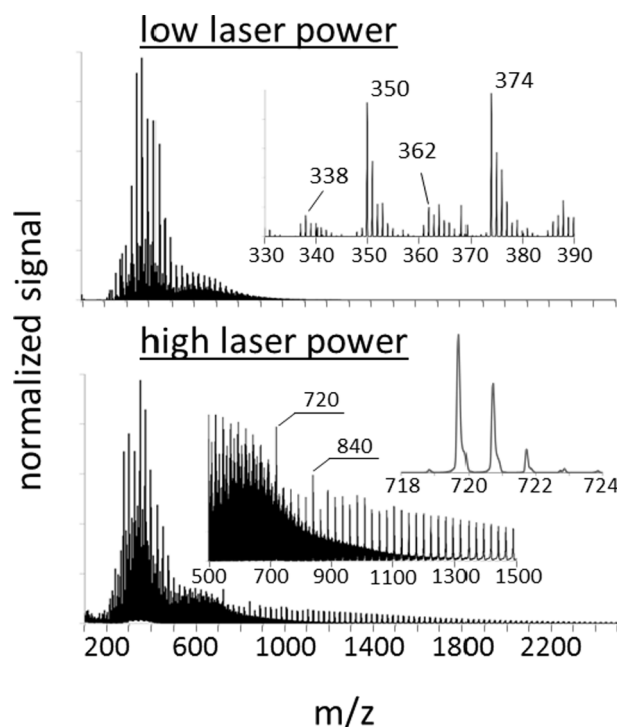Nevertheless, the striking effect of the high laser power is the

Fig. 4. Mass spectra of ethylene mature organic carbon at low (up) and high laser power (down).

appearance of a sequence of peaks spaced by m/z 24 appearing at $m/z >$ 500 and becoming evident for $m/z > 700$. This sequence is due to carbon clusters, whose stable structures arise above 26 carbon atoms [24] as demonstrated by: i) the higher peaks at m/z 720 and 840 typical of C_{60} and C_{70} fullerenes, ii) the mass peak difference of m/z 24 and iii) the typical isotopic fullerene distribution of the peaks [67], evidenced in the inset of the lower part of Fig. 4. The FFT and DBE analysis of mass spectra below reported has been carried out to infer more information on the features of the mass spectra of organic carbon and on the effect of high laser power.

3.2.1. FFT and DBE analysis: PAH and fullerene signatures.

The main features of the organic carbon spectra (Figs. 1 and 2) and the effect of laser power on molecular mass distribution (Fig. 4) are well highlighted by means of FFT analysis evidencing the periodic mass differences of mass spectra [43] (see experimental section). To take into account for

the change of the mass spectral distribution with increasing masses, the FFT analysis has been carried out in selected mass ranges.

Figure 5 reports an example of the height-normalized FFT profiles evaluated on the spectra of mature ethylene organic carbon measured at low and high laser power. Beside a mass spacing of 1 (indicating the presence of peaks at every mass unit), the 12 and 24 mass differences, typical of PAH growth sequences, appear predominant up to m/z 500, and become comparable in intensities up to m/z 1000. The repetitive 12 and 24 sequences observed at low laser power are still present at high laser power below m/z 500 and between m/z 500 and 1000, but the appearance above m/z 700 of the 24 mass difference, typical of carbon clusters, is remarkable. The FFT results can be better interpreted by comparing the FFT mass differences for organic carbon samples with those evaluated for other PAH-laden samples (PAH mixtures, asphaltenes and aromatic and aliphatic pitches) reported in Table 2, selected on the basis of their different aliphatic/aromatic character [45].

It is noteworthy that the 12 and 24 mass differences featuring organic carbon spectra (Table 2) characterize a PAH-rich sample like the aromatic pitch, derived from coal carbonization [45] involving the same molecular growth mechanism responsible for the occurrence of this sequence in flame-formed PAHs [51]. On the other hand, the 14 mass difference, indicative of methyl group substituents or methylene bridges between PAH units, feature asphaltenes and the aliphatic pitch in both laser power conditions, but it is not observed in the FFT analysis of organic carbon samples (Table 2).

These findings confirm the prevalent aromatic character of organic carbon as opposed to a negligible aliphaticity, either in terms of aliphatic substituents and/or aliphatic bridges between PAH moieties. Eventually, the tendency of high mass species to dehydrogenate is clearly evidenced by the stronger contribution of $m/z = 1$ mass difference in the high mass range of FFT profiles at high laser power (Fig. 5).

Further information on the aromaticity of organic carbon has been obtained from mass spectra by evaluation of the DBE, i.e. the unsaturation degree of hydrocarbons [44]. Fig. 6 reports the *iso*-abundance plot of the DBE number vs. CN evaluated on the mature organic carbon mass spectrum at low laser power, giving at a glance the extension of CN range and the unsaturation degree featuring organic carbon. The

relative abundance of each species has been evaluated as ratio of mass peak intensity to the sum intensity of all mass peaks and reported as dots of colour progressively lighter as the abundance decreases. Briefly, in the *iso*-abundance plot species having the same unsaturation degree but different carbon CN are characterized by the same DBE number (horizontal line), whereas species with different aromaticity of the core (different unsaturation degree) but the same CN present different DBE (vertical line). The width of the DBE distribution of mature organic carbon reported in Fig. 6 shows a DBE range narrower with respect to that typically evaluated for practical hydrocarbon samples as fossil fuels [68], and aliphatic (petroleum) pitches [45]. The low DBE width indicates a smaller variety of PAHs, similarly to aromatic (coal-derived) pitch [45]. Also the peculiarities of the even/odd carbon number sequences distribution above described (Fig. 4), are highlighted in the *iso*-abundance plot by: 1) higher intensity points (dark points) in the CN 20–40 range, associated to the even-C-numbered PAH sequence of the well-known stabilomer grid in the range m/z 300–522 [69] (see zoom of Fig. 6, and by 2) lighter points due to the odd-C-numbered PAH sequence [42,49]. The intensity of the points for CN > 40 progressively decreases and becomes low and undistinguishable for CN > 50–60.

Another DBE plot parameter related to structural factors is the slope of the line generated from the *iso*-abundance plot by connecting the maximum DBE numbers at given carbon numbers, named planar limit line (PLL) by Cho et al. [70]. At low laser power the PLL slope of 0.80, typical of PAHs [45], has been evaluated up to CN 100 (Fig. 6).

In comparison with the DBE plot evaluated at low laser power (Fig. 6), the *iso*-abundance plot at high laser power, reported in Fig. 7, extends toward higher carbon number (CN ≫100), splitting in two CN ranges because of the abrupt change of PLL slope and DBE at high carbon number (CN > 60–70). Specifically, the PLL slope of 0.80 observed for the organic carbon at low laser power (Fig. 6), is kept on up to CN = 60–70 (m/z 700–800) at high laser power (Fig. 7). Whereas in the CN 60–100 range, high intensity points due to all-carbon species appear, and the PLL slope assumes a value next to 1, typical of carbon clusters like fullerenes. For very high carbon number (CN > 100, m/z > 1200), only the sequence of high intensity points having regular differences of two carbon atoms is noticeable, confirming the prevalence of carbon
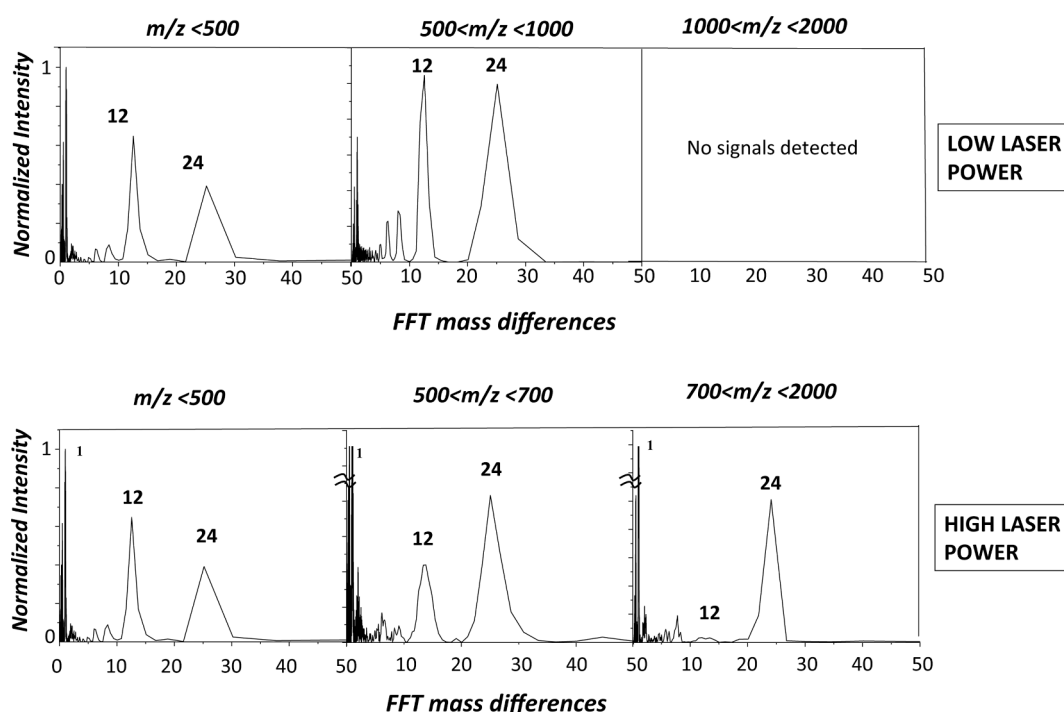

Fig. 5. Mass differences evaluated by FFT of mass spectra of mature organic carbon in different mass ranges at low (up) and high laser power (down).

Table 2
Mass differences evaluated by FFT analysis in different MS ranges of mass spectra of PAH-laden samples, young and mature soot at low and high laser power. In the last column, the indication of the carbon fullerene clusters occurrence at high laser power is reported (x). The numbers in bold indicate the higher intensity of the mass difference.

| PAH-laden samples	Mass difference m/z < 300	Mass difference m/z 300–500	Mass difference m/z 500–1000	Mass difference m/z 700–2000	Carbon clusters and fullerene occurrence
Organic carbon (young and mature)					
low laser power	**12**-24	**12**-24	12-24	–	-
high laser power	**12**-24	**12**-24	12-**24**	24	x
PAH (benzenoid and cyclopenta)					
low laser power			–	–	-
high laser power	–	–	24	24	x
Aromatic pitch					
low laser power	**12**–24	**12**–24	12–24	–	–
high laser power	**12**-24	**12**-24	12-**24**	24	x
Aliphatic pitch					
low laser power	14	14	14	–	–
high laser power	14	14	14	24	x
Asphaltenes					
low laser power	**12**–14	**12**–14	**12**–14	–	–
high laser power	**12**-14	**12**-14	**12**-14	24	x
SOOT	*m/z* (‹300)	*m/z* 300–380	*m/z* 380–700	*m/z* 700–2000	**Fullerene occurrence**
Young soot					
low laser power	12–**14**	–	12–**24**	–	–
high laser power	12-**14**	–	12-**24**	24	x
Mature soot					
low laser power	–	–	12–**24** (low)	–	–
high laser power	–	–	12-**24**	24 (low)	x (low)
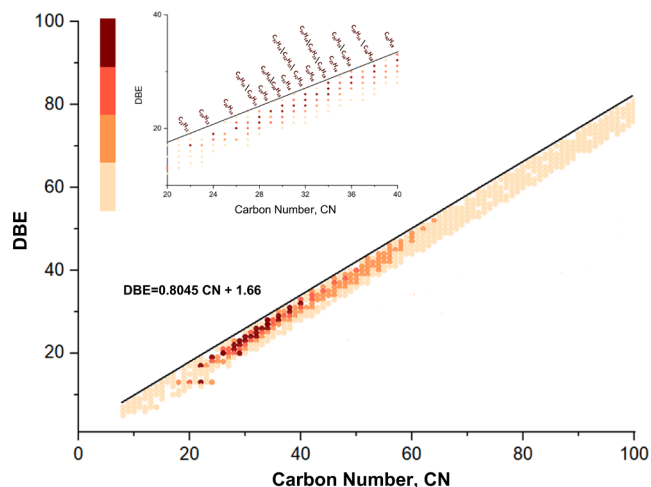
Fig. 6. Iso-abundance plot of DBE number vs. CN of hydrocarbon classes for mature ethylene organic carbon at low laser power. A zoom in the range of CN 20–40 is reported.

Fig. 7. Iso-abundance plots of DBE number vs. carbon number of hydrocarbon classes for mature ethylene organic carbon at high laser power. The color scale is normalized on the intensity maximum in the 10–180 CN range. The inset reports the zoom for the high CN species (100–180), with a color scale normalized on the intensity maximum in the high CN range.

clusters (inset of Fig. 7) evidenced also by FFT analysis above reported.

Definitely, the perusal of mass spectrometric data and FFT and DBE analysis of mass spectra at low and high laser power puts in evidence that in the LDI-TOFMS instrumental conditions used in this work, the laser power does not significantly affect the distribution of PAHs, still present in regular even and odd-C-number sequences with the predominance of even-C-numbered PAHs up to about *m/z* 500. The onset of fullerenes above *m/z* 500 and their predominance above *m/z* 1000 under high laser power conditions (lower part of Fig. 4 and Table 2) can be attributed to the enhancement of PAH vaporization and/or detachment causing a high concentration in the plume of PAHs reacting each other. Fullerene formation from PAHs likely follows the mechanism occurring in flames proposed by Homann [13,35] and Reilly [71], involving the reaction of two PAH molecules, or a molecule and a radical. As suggested by Homann [13,35], the peripheral hydrogen atoms of PAHs can be split off in a kind of concerted unimolecular zipper
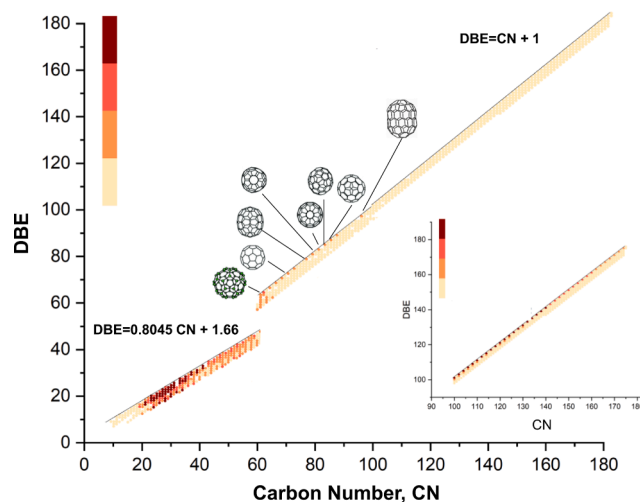
reaction, with the simultaneous shift of the pentagons into energetically favourable positions and closure of the necessary number of pentagons.

Overall, the occurrence of carbon clusters like fullerenes at high laser power can be attributed to artifacts, as also proposed in the case of asphaltenes and other carbonaceous materials [72–75]. The artifact source of fullerenes is confirmed by the effect of high laser power on LDI-TOFMS spectra of a mixture of fully-benzenoid and cyclopenta-PAHs (Table 2) presenting above *m/z* 500 a carbon cluster series featured by a mass difference of 24 (Table 2). Likewise, carbon cluster series, extended at higher masses (above *m/z* 700), can be observed in the mass spectra of PAH-laden samples as asphaltenes and pitches (Table 2). But, the sequence of carbon clusters is particularly evident in the mass spectrum of the aromatic pitch at high laser power reported in Fig. 8,
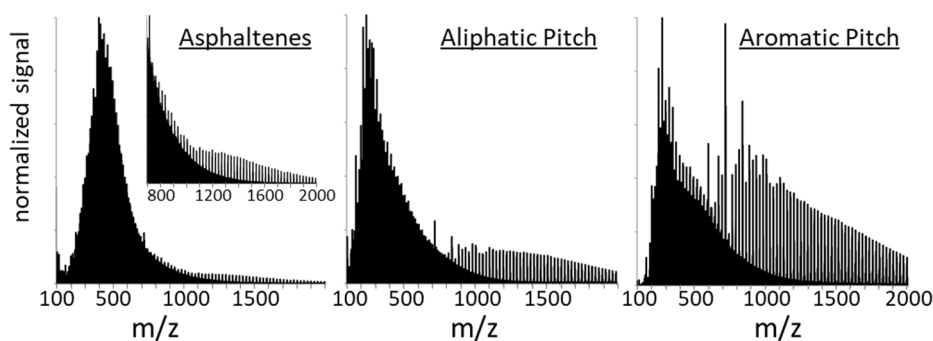
Fig. 8. Mass spectra at high laser power of: aromatic pitch (right), aliphatic pitch (center) and asphaltenes (left). Each spectrum is normalized on the maximum signal. The *m/z* 700–1000 region is zoomed in the inset of the left panel for evidencing the carbon cluster sequence.

compared to the mass spectra of asphaltenes and aliphatic pitch. This comparison confirms the higher propensity of unsubstituted PAHs as those constituting the aromatic pitch [45], to form carbon clusters in respect to alkyl-substituted PAHs mainly featuring asphaltenes and aliphatic pitch [45].

3.2.2. The effect of laser power on the organic carbon mass distribution.
Consistently with LDI-TOFMS results [31], the persistence upon high laser power of the second mass distribution mode (*m/z* 500–1000) (Fig. 4), along with the similarity of FFT features with those of the other PAH-laden samples (Table 2) hint to exclude the contribution of aliphatic moieties recently suggested by tandem MS [66] and laser induced fluorescence [56]. The persistence under high laser power of the second mode of mass distribution, featured by the 12 and 24 sequences typical of PAHs (Table 2), strengthens the attribution of high mass species to large PAHs rather than to PAH dimers or alkylated PAHs. This inference is supported by the LDI-TOFMS analysis of aromatic and aliphatic pitch at low and high laser power contrasted in Fig. 9 and Fig. 10, respectively.

As matter of fact, the organic carbon behaves similarly to the aromatic pitch, undergoing just some fragmentation for effect of the laser power (Fig. 4), whereas in the aliphatic pitch constituted of alky-substituted PAH oligomers (mainly dimers) [76,77] the main mode, almost peaked around *m/z* 500, significantly decreases to benefit of lower mass species peaked around *m/z* 250 (Fig. 10).

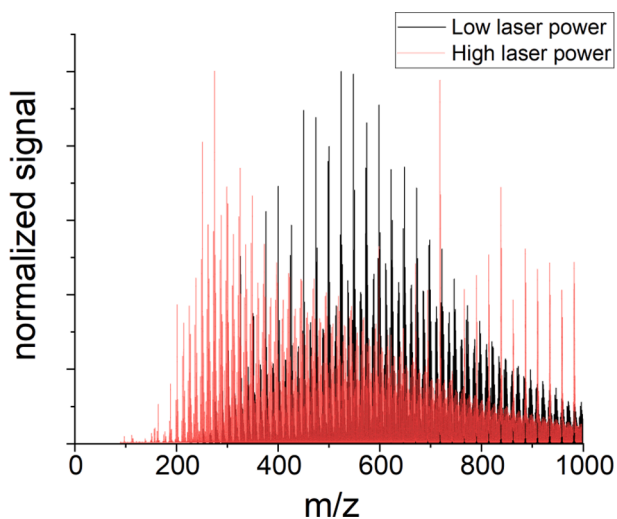It has to be underlined that the negligible or no formation of PAH

Fig. 10. Mass spectra at low (black) and high laser power (red) of aliphatic pitch. The spectra are normalized on the maximum signal. (For interpretation of the references to color in this figure legend, the reader is referred to the web version of this article.)
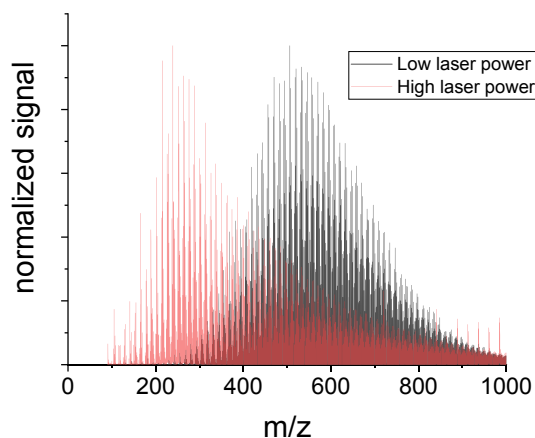
dimers inferred from the LDI-TOFMS data so far described, does not exclude the possibility of the formation of small dimers, not falling in the mass range investigated, as those coming from reactive dimerization of one-ring aromatics. Kholghy et al. [65] have computed that one-ring aromatic species like benzene, toluene, phenylacetylene, give the major contribution to dimer formation and soot loading. Indeed, this framework well justifies also the sudden soot formation in benzene flames occurring so quickly already in the oxidation region where one-ring aromatic radicals and species are abundantly present [30], that the PAH growth is prevented.

3.3. Soot

The analysis of LDI-TOF mass spectra of soot is quite challenging given the complexity and the general "inertness" of carbon solids as soot to ionization and fragmentation, and hence the difficulty to produce reliable mass spectral data. However, preliminary results on LDI-TOFMS analysis of soot here reported clearly show how much different soot is in comparison to organic carbon questioning all the interpretations of soot inception merely based on the analysis of whole carbon PM. The phenomenon most under study in soot formation process is just soot inception, i.e. the transition from molecular to the solid phase featuring the first soot particles. Consistently, what is meant for soot in this work is the insoluble (solid) component of carbon PM obtained by DCM extraction of organic carbon. Actually, soot particles are insoluble in all solvents, but, similarly to some carbon materials as carbon black and coal, they can be generally suspended in powerful solvents as NMP, allowing the determination of molecular weight distribution [78] and

Fig. 9. Mass spectra at low (black) and high laser power (red) of aromatic pitch. The spectra are normalized on the maximum signal. (For interpretation of the references to color in this figure legend, the reader is referred to the web version of this article.)

spectroscopic features as the mass absorption coefficient (MAC) [8] and optical band gap [9].

Some differences in the mass spectral behaviour were expected for soot sampled at inception and at the end of the soot formation process on the basis of different soot properties like H/C and MAC, observed as a function of soot aging and fuel [8,30]. Indeed, LDI-TOFMS analysis at low laser power resulted to be negligibly or no effective in producing reliable and significant mass spectrometric signals especially from mature soot. Young soot coming from hydrogen-rich fuels as methane and ethylene makes exception showing some tendency in fragmenting and producing radicals detectable by LDI-TOFMS at low laser power.

As an example, Fig. 11 reports the mass spectrum of young ethylene soot measured at low laser power. The mass spectrum in Fig. 11 presents peaks at odd masses in the low molecular mass region (m/z ⟨300⟩, likely due to radical species. The FFT analysis carried out on soot mass spectra (Table 2) puts in evidence the occurrence of mass differences of 12 and 14, with prevalence of 14. Interestingly enough, the 14 difference can be traceable to homologue series increasing by a CH_2 group (structures with aliphatic moieties as those featuring C_5-PAHs like fluorene, cyclopentaphenanthrene, and so on). Above m/z 500 the FFT mass differences become 12 and 24 with prevalence of 24 (Table 2), indicating the presence of carbon clusters not ascribable, however, to the typical fullerene cluster series.

The LDI-TOFMS spectra of young ethylene and benzene soot at high laser power are reported in Fig. 12. Beside to increase the ion yield from ethylene young soot in the low mass region (<m/z 300), the high laser power was found to be effective in producing mass spectral signals in the case of benzene young soot. In this low mass range the same FFT mass differences of 12 and 14 found for young soot at low laser power have been evaluated (Table 2), whereas the production of carbon clusters in the high mass region (>m/z 500) with mass difference of 12 and 24 up to about m/z 600–700 is remarkable (with prevalent 24 mass difference, Table 2. Above m/z 600–700 only the mass difference of 24 can be noticed, but in this case the predominance of m/z 720 and 840, ascribed to C_{60} and C_{70} fullerenes, is evident. It is confirmed by the DBE vs CN graph reported in Fig. S3 in the Supplementary Material, where high intensity points due to all-carbon species appear in the CN > 60 range, and the PLL slope assumes a value next to 1, typical of carbon clusters like fullerenes.

With regard to mature soot, a generally low signal intensity and slight signals, mainly due to carbon clusters above m/z 500, could be
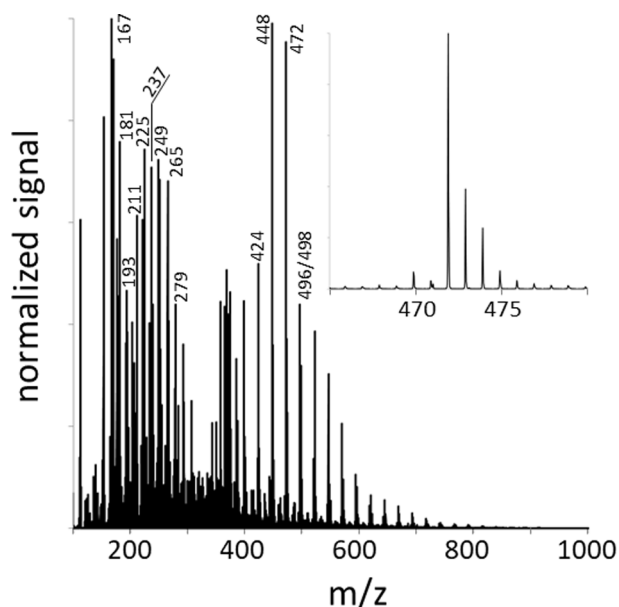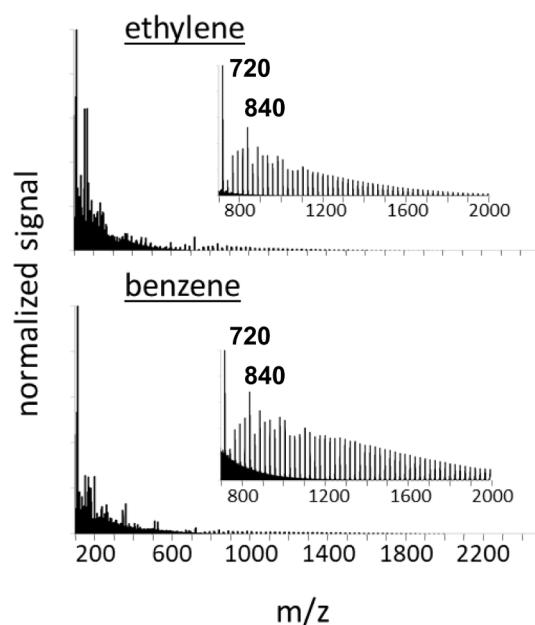

Fig. 12. Mass spectra of young ethylene (up) and benzene (down) soot at high laser power.

detected only at high laser power (Table 2). The LDI-TOFMS analysis ineffectiveness on mature soot, even under high laser power conditions, reflects a structural change from the amorphous-like network of young soot to a more inert turbostratic structure featuring mature soot.

In previous works carbon clusters and fullerene ions have been detected in soot particle mass spectra [21,22,79–80] and their presence has been correlated with the refractory organic carbon more than to the refractory carbon [22,39]. Since soot samples here analysed are devoid of organic carbon (not-refractory organic carbon), fullerenes may come from ablation of aromatics not extractable with DCM (refractory organic carbon) somehow very strictly linked to soot network [9,21,23], or can originate from fullerene-like moieties of the carbon network [80]. The higher fullerene signal was detected in the case of young soot (Table 2) that presents shorter and more tortuous fringes in the nanostructure and higher heterogeneity and lower sp^2 content, possibly due to cyclopenta-containing aromatic species on the border of soot particles, as demonstrated by EELS [81]. That the higher propensity of ethylene and methane young soot to form fullerenes could be related to the nanostructure is supported by TEM imaging of young soot. The TEM image reported in Fig. 13 shows that upon laser annealing [81], ethylene young soot forms hollow shell structures with internal voids, similar to big fullerene-like structures, as occurs in the case of fullerenic carbon [80,82]. As soot ages the low and/or negligible radical and fullerene formation can be related to the increase of the turbostratic character of
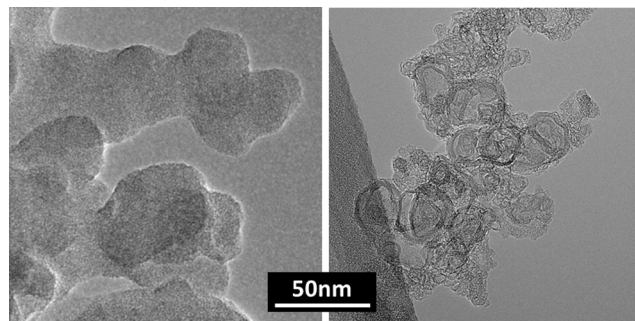

Fig. 11. Mass spectrum at low laser power of young ethylene soot.

Fig. 13. TEM images of ethylene young soot before (left) and after laser interaction (right).

soot [81], quite stable and less prone to undergo significant fragmentation and breaking. In future work, the correlation between soot nanostructure and mass spectra behaviour will be inferred by implementing the LDI-TOFMS analytical approach on a large number of young and mature soot samples coming from different experimental conditions in comparison with subsets of refractory carbons with either fullerenic, turbostratic or graphitic networks.

Eventually, with regard to the organic carbon and soot interrelationship and implications to soot formation, their quite different mass spectra demonstrate that organic carbon and soot do not have common chemical features directly relating each to other.

First, the most significant difference between organic carbon and young soot is the complete absence of mass peaks due to PAH molecules/radicals in the mass spectra of soot, even of young soot. It derives that the fringes identified by TEM in the soot nanostructure and attributed to polyaromatic ring moieties should be so crosslinked each other in a turbostratic way to hinder their "withdrawal" from carbon network even under high laser power. The compositional and structural motif differences between organic carbon and soot demonstrate that the distinction between these two components of carbon PM is important especially for inferring the not yet untangled transition from molecular to solid phase featuring soot inception. In other words, since organic carbon generally dominates the whole PM mass spectrum, the direct analysis of whole carbon PM leads to misleading results as regards soot structure and inception mechanism. Actually, the results obtained by LDI-TOFMS analysis of organic carbon and soot from premixed flames producing particulate matter with high (methane and ethylene flames) and low (benzene flame) organic carbon/soot ratio have some implications to soot formation mechanism.

Figure 14 aims to schematize PAH and soot formation and growth built on the basis of the mass spectra of young and mature soot at low and high laser power, respectively. The upper route starts from a globular coalesced material, typically found at inception in the fuel-rich aliphatic premixed flames as those here studied [81], and in form of PAH-containing particles inside diffusion flames [16,83,84]. Remembering that organic carbon is abundantly present along the aliphatic fuel flames, the spectra of the organic carbon have been also reported in Fig. 14, above the spectra of methane and ethylene soot, to put in evidence how different organic carbon is in comparison to both young and mature soot. As before underlined, organic carbon spectra show the predominance of PAHs, mainly composed of pericondensed six-rings up to C40 in the young organic carbon, which slightly grow as soot ages undergoing some enrichment in second mode from C40 to C60, the latter one likely composed of a mixture of six-ring and C$_5$-PAHs. Young soot is relatively reactive and prone to form small hydrocarbon radicals and carbon clusters. Dehydrogenation/carbonization as soot ages is testified by the very low mass signals detected even at high laser power.

On the opposite, the PAH and soot formation route from the benzene flame, shown in the lower part of Fig. 14, seems not to involve PAH growth implying the occurrence of reactive coagulation and clustering of small aromatic radicals [65,84] directly producing young aciniform soot particles [81,85] where aromatic motifs, crosslinked each other, are likely to eject radicals and form some fullerenes, especially under high laser power.

The two paths are not mutually exclusive and can cross each other in dependence on the pool of species/radicals, in turn depending on the hydrocarbon fuel, temperature and C/O feed conditions [86]. Summarizing, PAH formation precedes and/or accompanies soot formation, somehow contributing to soot coagulation and aggregation. When a huge number of small aromatic radicals are early available in the oxidation region of the flame as often occurs in the case of aromatic flames, they can directly react forming soot particles whose physical and chemical features do not significantly change going from young to mature soot [87].

4. Conclusions

The main focus of the work was on the mass spectral characterization by LDI-TOFMS of young and mature organic carbon, extracted from carbon PM thermophoretically deposited, respectively, at the beginning and at the end of the soot formation region of hydrocarbon fuels premixed flames (methane, ethylene and benzene). The perusal of mass spectra of young and mature organic carbon at low and high laser power in comparison to those of PAH-laden samples and eventually to soot, put in evidence the organic carbon features and differences between organic carbon and soot, the latter one showing a significant inertness to LDI-TOFMS analysis.

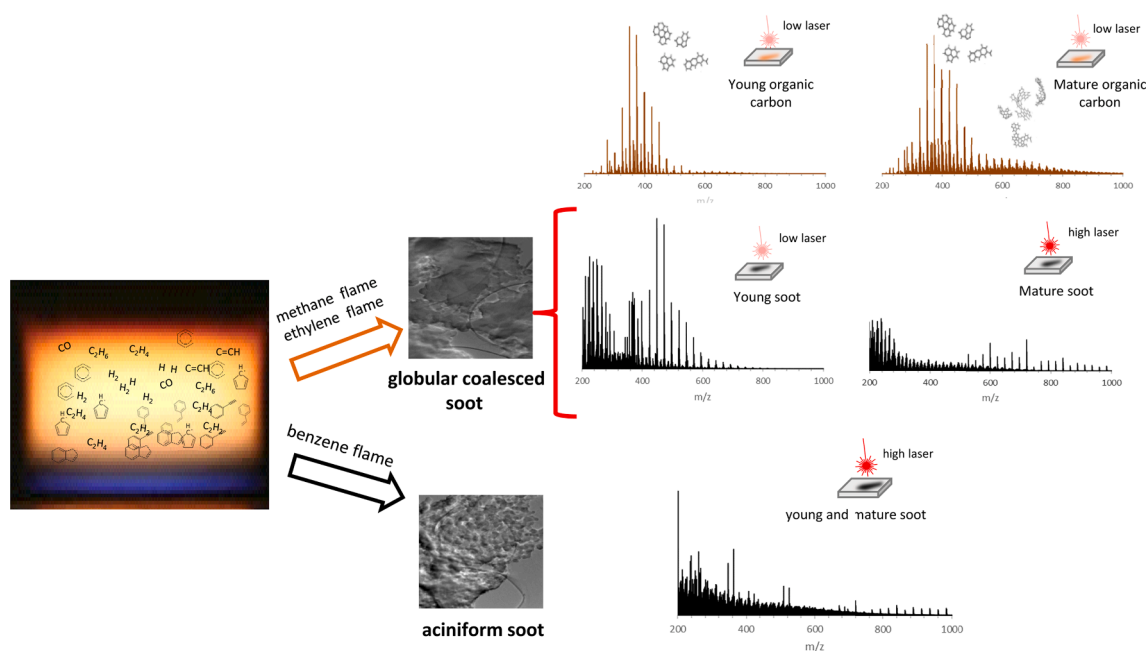In particular with regard to organic carbon it was found that:

Fig. 14. Schematic view of PAH and soot formation built up on the basis of mass spectra of young and mature organic carbon and soot.

- Organic carbon, abundantly present in methane and ethylene flames, exhibited a similar bimodality of mass spectra measured at low laser power, with a trough at m/z 500 delimiting a low mass region, where even-C-numbered PAHs prevail on odd-C-numbered PAHs, from a high-mass region extending up to about m/z 1000, enriched in odd-C-numbered PAHs like cyclopenta-substituted PAHs. The second high-mass mode was more evident for mature organic carbon, testifying the occurrence of some molecular growth as soot ages. Organic carbon formed in the benzene flame was not analysable by LDI-TOFMS due to the low available amounts along with the abundance of oxygen-containing species (phenols) and the low contribution of PAHs.

- LDI-TOFMS analysis of organic carbon carried out with high laser power showed some PAH dehydrogenation and radical formation not significantly modifying the mass spectral shape, namely its bimodality. The persistence of the second mode under high laser power led to the attribution of high masses to stable large PAH and radicals, rather than to dimers, aliphatically-bridged or alkyl-substituted PAHs. This inference was confirmed by the perusal of LDI-TOFMS spectra of organic carbon in comparison with those measured for PAH-laden samples like aromatic and aliphatic pitches, and asphaltenes. Also fullerene formation from organic carbon seemed correlated with the aromaticity, namely organic carbon and aromatic pitch showed higher fullerene formation under high laser power in comparison to asphaltenes and aliphatic pitch.

With regard to soot, it has been shown that:

LDI-TOFMS analysis of the soot component of carbon PM resulted to be effective only for ethylene and methane young soot, showing peaks at odd masses in the low molecular mass region ($m/z < 300$) likely due to radicals and carbon clusters mainly spaced by 24 above m/z 380–400. As matter of fact, the FFT analysis of young soot mass spectrum put in evidence the occurrence of mass difference of 12–14 among the $m/z < 300$ peaks, with prevalence of 14 mass difference possibly due to aliphatic CH_2 groups like those featuring cyclopenta-containing aromatic moieties. Above m/z 400 the mass difference becames 12–24 with large prevalence of 24 mass difference, typical of carbon cluster series.

Few information on mature soot could be obtained only at high laser power. As in the case of organic carbon, the main effect of high laser power regarded the appearance of carbon clusters series spaced by m/z 24 where C_{60}, C_{70} fullerenes could be identified.

Eventually, caution should be employed for interpreting LDI-TOF mass spectra, in particular when high laser power is employed because of the artifact formation. However, the work demonstrates that the different response to laser ionization as well as the formation of specific artifacts are proofs of the quite different composition of organic carbon and soot. Such differences are helpful for well discriminating organic carbon from soot and evidence the importance of discriminating between them, especially if insights into the formation of the soot are to be obtained.

Further work will be devoted to analyze the correlation between soot nanostructure and mass spectra behaviour of young and mature soot samples in comparison with subsets of refractory carbons with either fullerenic, turbostratic or graphitic networks.

CRediT authorship contribution statement

B. Apicella: Conceptualization, Data curation, Investigation, Supervision, Writing – original draft, Writing – review & editing. **C. Russo:** Data curation, Investigation, Writing – review & editing. **A. Carpentieri:** Investigation. **A. Tregrossi:** Data curation, Investigation. **A. Ciajolo:** Conceptualization, Writing – review & editing.

Declaration of Competing Interest

The authors declare that they have no known competing financial interests or personal relationships that could have appeared to influence the work reported in this paper.

Appendix A. Supplementary data

Supplementary data to this article can be found online at https://doi.org/10.1016/j.fuel.2021.122356.

References

[1] Niranjan R, Thakur AK. The toxicological mechanisms of environmental soot (black carbon) and carbon black: focus on oxidative stress and inflammatory pathways. Front Immunol 2017;8:763. https://doi.org/10.3389/fimmu.2017.00763.

[2] Lohmann U, Friebel F, Kanji ZA, Mahrt F, Mensah AA, Neubauer D. Future warming exacerbated by aged-soot effect on cloud formation. Nat Geosci 2020;13 (10):674–80. https://doi.org/10.1038/s41561-020-0631-0.

[3] Bond TC, Doherty SJ, Fahey DW, Forster PM, Berntsen T, DeAngelo BJ, Flanner MG, Ghan S, Kärcher B, Koch D, Kinne S. Bounding the role of black carbon in the climate system: a scientific assessment. J Geophys Res Atmos 2013; 118(11): 5380-5552. 10.1002/jgrd.50171.

[4] Homann KH, Wagner HG. Some new aspects of the mechanism of carbon formation in premixed flames. Proc Combust Inst 1967;11(1):371–9. https://doi.org/10.1016/S0082-0784(67)80161-9.

[5] Haynes BS, Wagner HG. Wagner, soot formation. Prog Energy Combust Sci 1981;7 (4):229–73. https://doi.org/10.1016/0360-1285(81)90001-0.

[6] Richter H, Howard JB. Formation of polycyclic aromatic hydrocarbons and their growth to soot—a review of chemical reaction pathways, Prog Energy Combust Sci 26 (2000) 565–608. 10.1016/S0360-1285(00)00009-5.

[7] Dobbins RA, Fletcher RA, Chang H-C. The evolution of soot precursor particles in a diffusion flame. Combust Flame 1998;115(3):285–98. https://doi.org/10.1016/S0010-2180(98)00010-8.

[8] Apicella B, Alfè M, Barbella R, Tregrossi A, Ciajolo A. Aromatic structure of carbonaceous materials and soot inferred by spectroscopic analysis. Carbon 2004; 42:1583–9. https://doi.org/10.1016/j.carbon.2004.02.010.

[9] Russo C, Apicella B, Lighty JS, Ciajolo A, Tregrossi A. Optical properties of organic carbon and soot produced in an inverse diffusion flame. Carbon 2017;124:372–9. https://doi.org/10.1016/j.carbon.2017.08.073.

[10] Cleon G, Amodeo T, Faccinetto A, Desgroux P. Laser induced incandescence determination of the ratio of the soot absorption functions at 532 nm and 1064 nm in the nucleation zone of a low pressure premixed sooting flame. Appl Phys B 2011; 104:297–305. https://doi.org/10.1007/s00340-011-4372-z.

[11] López-Yglesias X, Schrader PE, Michelsen HA. Soot maturity and absorption cross sections. J Aerosol Sci 2014;75:43–64. https://doi.org/10.1016/j.jaerosci.2014.04.011.

[12] Lapuerta M, Rodríguez-Fernández J, Sánchez-Valdepeñas J. Soot reactivity analysis and implications on diesel filter regeneration. Prog Energy Combust Sci 2020;78: 100833. https://doi.org/10.1016/j.pecs.2020.100833.

[13] Bachmann M, Wiese W, Homann KH. Thermal and chemical influences on the soot mass. Proc Combust Inst 1994:635–43. https://doi.org/10.1016/S0082-0784(06)80695-8.

[14] Skeen SA, Michelsen HP, Wilson KR, Popolan DM, Violi A, Hansen N. Near-threshold photoionization mass spectra of combustion-generated high-molecular-weight soot precursors. J Aerosol Sci 2013;58:86–102. https://doi.org/10.1016/j.jaerosci.2012.12.008.

[15] Homann K-H. Fullerenes and soot formation: new pathways to large particles in flames. Angew Chem 1998;37(18):2434–51. https://doi.org/10.1002/(SICI)1521-3773(19981002)37:18<2434::AID-ANIE2434>3.0.CO;2-L.

[16] Reilly PTA, Gieray RA, Whitten WB, Ramsey JM. Direct observation of the evolution of the soot carbonization process in an acetylene diffusion flame via real-time aerosol mass spectrometry. Combust Flame 2000;122(1-2):90–104. https://doi.org/10.1016/S0010-2180(00)00105-X.

[17] Faccinetto A, Desgroux P, Ziskind M, Therssen E, Focsa C. High-sensitivity detection of polycyclic aromatic hydrocarbons adsorbed onto soot particles using laser desorption/laser ionization/time-of-flight mass spectrometry: an approach to studying the soot inception process in low-pressure flames. Combust Flame 2011; 158(2):227–39. https://doi.org/10.1016/j.combustflame.2010.08.012.

[18] Ngo LD, Duca D, Carpentier Y, Noble JA, Ikhenazene R, Vojkovic M, et al. Chemical discrimination of the particulate and gas phases of miniCAST exhausts using a two-filter collection method. Atmos Meas Tech 2020;13(2):951–67. https://doi.org/10.5194/amt-13-951-2020.

[19] Faccinetto A, Focsa C, Desgroux P, Ziskind M. Progress toward the quantitative analysis of PAHs adsorbed on soot by laser desorption/laser ionization/time-of-flight mass spectrometry. Environ Sci Technol 2015;49(17):10510–20. https://doi.org/10.1021/acs.est.5b02703.

[20] Irimiea C, Faccinetto A, Mercier X, Ortega IK, Nuns N, Therssen E, et al. Unveiling trends in soot nucleation and growth: when secondary ion mass spectrometry

meets statistical analysis. Carbon 2019;144:815–30. https://doi.org/10.1016/j.carbon.2018.12.015.

[21] Maricq MM. An examination of soot composition in premixed hydrocarbon flames via laser ablation particle mass spectrometry. J Aerosol Sci 2009;40(10):844–57. https://doi.org/10.1016/j.jaerosci.2009.07.001.

[22] Matti Maricq M. Examining the relationship between black carbon and soot in flames and engine exhaust. Aerosol Sci Technol 2014;48(2014):620–9. https://doi.org/10.1080/02786826.2014.904961.

[23] Malmborg VB, Eriksson AC, Török S, Zhang Y, Kling K, Martinsson J, et al. Relating aerosol mass spectra to composition and nanostructure of soot particles. Carbon 2019;142:535–46. https://doi.org/10.1016/j.carbon.2018.10.072.

[24] Pino T, Chabot M, Béroff K, Godard M, Fernandez-Villoria F, Le KC, et al. Release of large polycyclic aromatic hydrocarbons and fullerenes by cosmic rays from interstellar dust. Swift heavy ion irradiations of interstellar carbonaceous dust analogue. Astron Astrophis 2019;623:A134. https://doi.org/10.1051/0004-6361/201834855.

[25] Bonnin MA, Falvo C, Calvo F, Pino T, Parneix P. Simulating the structural diversity of carbon clusters across the planar-to-fullerene transition. Phys Rev A 2019;99:042504. https://doi.org/10.1103/PhysRevA.99.042504.

[26] Violi A, Sarofim AF, Truong TN. Mechanistic pathways to explain H/C ratio of soot precursors. Combust Sci Technol 2002;174(11-12):205–22.

[27] Carbone F, Gleason K, Gomez A. Probing gas-to-particle transition in a moderately sooting atmospheric pressure ethylene/air laminar premixed flame. Part I: gas phase and soot ensemble characterization. Combust Flame 2017; 181: 315-28. https://doi.org 0.1016/j.combustflame.2017.01.029.

[28] Baldelli A, Trivanovic U, Sipkens TA, Rogak SN. On determining soot maturity: a review of the role of microscopy-and spectroscopy-based techniques. Chemosphere 2020;252:126532. https://doi.org/10.1016/j.chemosphere.2020.126532.

[29] C. Russo, A. Tregrossi, A. Ciajolo, Dehydrogenation and growth of soot in premixed flames, Proc Combust Inst 2015; 35(2): 1803-1809. 10.1016/j.proci.2014.05.024.

[30] Zhang W, Shao C, Sarathy SM. Analyzing the solid soot particulates formed in a fuel-rich flame by solvent-free matrix-assisted laser desorption/ionization Fourier transform ion cyclotron resonance mass spectrometry. Rapid Commun Mass Spectrom 2019;34:e8596. https://doi.org/10.1002/rcm.8596.

[31] Jacobson RS, Korte AR, Vertes A, Miller JH. The molecular composition of soot. Angew Chem 2019;132:14115. https://doi.org/10.1002/ange.201914115.

[32] Schulz F, Commodo M, Kaiser K, De Falco G, Minutolo P, Meyer G, et al. Insights into incipient soot formation by atomic force microscopy. Proc Combust Inst 2019; 37(1):885–92. https://doi.org/10.1016/j.proci.2018.06.100.

[33] Apicella B, Alfè M, Amoresano A, Galano E, Ciajolo A. Advantages and limitations of laser desorption/ionization mass spectrometric techniques in the chemical characterization of complex carbonaceous materials. Int J Mass Spec 2010;295(1-2):98–102. https://doi.org/10.1016/j.ijms.2010.06.022.

[34] Pontier Johnson M, Donnet JB, Wang TK, Wang CC, Locke RW, Brinson BE, Marriott T. A dynamic continuum of nanostructured carbons in the combustion furnace, Carbon 2002; 40(2): 189-194. 10.1016/S0008-6223(01)00172-5.

[35] Ahrens J, Bachmann M, Baum Th, Griesheimer J, Kovacs R, Weilmünster P, et al. Fullerenes and their ions in hydrocarbon flames. Intern J Mass Spectrom Ion Proc 1994;138:133–48. https://doi.org/10.1016/0168-1176(94)04036-2.

[36] Russo C, Apicella B, Tregrossi A, Oliano MM, Ciajolo A. Thermophoretic sampling of large PAH (C≥22–24) formed in flames. Fuel 2020;263:116722. https://doi.org/10.1016/j.fuel.2019.116722.

[37] Atiku FA, Mitchell EJS, Lea-Langton AR, Jones JM, Williams A, Bartle KD. The impact of fuel properties on the composition of soot produced by the combustion of residential solid fuels in a domestic stove. Fuel Process Technol 2016;151:117–25. https://doi.org/10.1016/j.fuproc.2016.05.032.

[38] Apicella B, Tregrossi A, Popa C, Mennella V, Ciajolo A, Russo C. Study on the separation and thin film deposition of tarry aromatics mixtures (soot extract and naphthalene pitch) by high-vacuum heating. Fuel 2017;201:118–23. https://doi.org/10.1016/j.fuel.2017.08.014.

[39] Corbin JC, Sierau B, Gysel M, Laborde M, Keller A, Kim J, et al. Mass spectrometry of refractory black carbon particles from six sources: carbon-cluster and oxygenated ions. Atmos Chem Phys 2014;14(5):2591–603. https://doi.org/10.5194/acp-14-2591-2014.

[40] Przybilla L, Brand JD, Yoshimura K, Rader HJ, Müllen K. MALDI-TOF mass spectrometry of insoluble giant polycyclic aromatic hydrocarbons by a new method of sample preparation. Anal Chem 2000;72:4591.4597. https://doi.org/10.1021/ac000372q.

[41] Rizzi A, Cosmina P, Flego C, Montanari L, Seraglia R, Traldi P. Laser desorption/ionization techniques in the characterization of high molecular weight oil fractions. Part 1: asphaltenes. J Mass Spectrom 2006;41(9):1232–41. https://doi.org/10.1002/jms.1095.

[42] Apicella B, Carpentieri A, Alfè M, Barbella R, Tregrossi A, Pucci P, et al. Mass spectrometric analysis of large PAH in a fuel-rich ethylene flame. Proc Comb Inst 2007;31(1):547–53. https://doi.org/10.1016/j.proci.2006.08.014.

[43] Apicella B, Bruno A, Wang X, Spinelli N. Fast Fourier Transform and autocorrelation function for the analysis of complex mass spectra. Int J Mass Spectrom 2013;338:30–8. https://doi.org/10.1016/j.ijms.2013.01.003.

[44] Pellegrin V. Molecular formulas of organic compounds: the nitrogen rule and degree of unsaturation. J Chem Educ 1983;60(8):626–33. https://doi.org/10.1021/ed060p626.

[45] Zhang W, Andersson JT, Rader HJ, Müllen K. Molecular characterization of large polycyclic aromatic hydrocarbons in solid petroleum pitch and coal tar pitch by high resolution MALDI TOF MS and insights from ion mobility separation. Carbon 2015;95:672–80. https://doi.org/10.1016/j.carbon.2015.08.057.

[46] Wetzel S, Guttman CM, Girard JE. The influence of laser energy of MALDI on the molecular mass distribution of synthetic polymers. J Res Natl Stand Technol 2001; 42.

[47] Beck MT, Kéki S, Szabó PT, Zsuga M. Comparative study of carbonization of hydrocarbons. The 24-26 rule. Tetrahedron, 1999; 55(6): 1799-1806. 10.1016/S0040-4020(98)01192-2.

[48] Lafleur AL, Taghizadeh K, Howard JB, Anacleto JF, Quilliam MA. Characterization of flame-generated C10 to C160 polycyclic aromatic hydrocarbons by atmospheric-pressure chemical ionization mass spectrometry with liquid introduction via heated nebulizer interface. J Am Soc Mass Spectrom 1996;7(3):276–86. https://doi.org/10.1016/1044-0305(95)00651-6.

[49] Siegmann K, Hepp H, Sattler K. Reactive dimerization: a new PAH growth mechanism in flames. Combust Sci Technol 1995;109(1–6):165–81. https://doi.org/10.1080/00102209508951900.

[50] Cain J, Laskin A, Kholghy MR, Thomson MJ, Wang H. Molecular characterization of organic content of soot along the centerline of a coflow diffusion flame. Phys Chem Chem Phys 2014;16(47):25862–75. https://doi.org/10.1039/C4CP03330B.

[51] Keller A, Kovacs R, Homann KH. Large molecules, ions, radicals and small soot particles in fuel-rich hydrocarbon flames. Phys Chem Chem Phys 2000;2:1667–75. https://doi.org/10.1039/A908190I.

[52] Panariello M, Apicella B, Armenante M, Bruno A, Ciajolo A, Spinelli N. Analysis of polycyclic aromatic hydrocarbon sequences in a premixed laminar flame by on-line time-of-flight mass spectrometry. Rapid Commun Mass Spectrom 2008;22(4):573–81. https://doi.org/10.1002/rcm.3391.

[53] Stone AJ, Wales DJ. Theoretical studies of icosahedral C₆₀ and some related species. Chem Phys Lett 1986;128:501–3. https://doi.org/10.1016/0009-2614(86)80661-3.

[54] Scott LT. Fragments of fullerenes: novel syntheses, structures and reactions. Pure Appl Chem 1996;68(2):291–300. https://doi.org/10.1351/pac199668020291.

[55] Lafleur AL, Howard JB, Taghizadeh K, Plummer EF, Scott LT, Necula A, et al. Identification of $C_{20}H_{10}$ dicyclopentapyrenes in flames: correlation with corannulene and fullerene formation. J Phys Chem 1996;100(43):17421–8. https://doi.org/10.1021/jp9605313.

[56] Mercier X, Carrivain O, Irimiea C, Faccinetto A, Therssen E. Dimers of polycyclic aromatic hydrocarbons: the missing pieces in the soot formation process. Phys Chem Chem Phys 2019;21(16):8282–94.

[57] Bachmann M, Wiese W, Homann K-H. PAH and aromers: Precursors of fullerenes and soot. Proc Combust Instit 1996;26:2259.

[58] Miller JH. The kinetics of polynuclear aromatic hydrocarbon agglomeration in flames. Symp (Int) Combust 1991;23(1):91–8.

[59] Herdman JD, Miller JH. Intermolecular potential calculations for polynuclear aromatic hydrocarbon clusters. J Phys Chem A 2008;112(28):6249–56.

[60] Schuetz CA, Frenklach M. Nucleation of soot: molecular dynamics simulations of pyrene dimerization. Proc Combust Inst 2002;29(2):2307–14.

[61] Totton TS, Misquitta AJ, Kraft M. A quantitative study of the clustering of polycyclic aromatic hydrocarbons at high temperatures. Phys Chem Chem Phys 2012;14(12):4081. https://doi.org/10.1039/c2cp23008a.

[62] Sabbah H, Biennier L, Klippenstein SJ, Sims IR, Rowe BR. Exploring the role of PAHs in the formation of soot: pyrene dimerization. J Phys Chem Lett 2010;1:2962–7.

[63] Eaves NA, Dworkin SB, Thomson MJ. Assessing relative contributions of PAHs to soot mass by reversible heterogeneous nucleation and condensation. Proc Combust Inst 2017;36(1):935–45.

[64] Kholghy M, Eaves NA, Veshkini A, Thomson MJ. The role of "chemical bond formation" in reducing soot nucleation reversibility. Proc Combust Inst 2019;37:1003–11.

[65] Kholghy MR, Kelesidis GA, Pratsinis SE. Reactive polycyclic aromatic hydrocarbon dimerization drives soot nucleation, Phys. Chem. Chem. Phys. 2018; 20: 10926e10938, 10.1039/C7CP07803J.

[66] Adamson BD, Skeen SA, Ahmed M, Hansen N. Detection of aliphatically bridged multi-core polycyclic aromatic hydrocarbons in sooting flames with atmospheric-sampling high-resolution tandem mass spectrometry. J Phys Chem A 2018;122 (48):9338–49.

[67] Martin JW, McIntosh GJ, Arul R, Oosterbeek RN, Kraft M, Söhnel T. Giant fullerene formation through thermal treatment of fullerene soot, Carbon, 125 (2017) 132-138. https://doi.org/10.1016/j.carbon.2017.09.045.

[68] Niyonsaba E, Manheim JM, Yerabolu R, Kenttämaa HI. Recent advances in petroleum analysis by mass spectrometry. Anal Chem 2019;91(1):156–77. https://doi.org/10.1021/acs.analchem.8b05258.

[69] Fahr A, Stein SE. Reactions of vinyl and phenyl radicals with ethyne, ethene and benzene. Proc Comb Inst 1989;22(1):1023–9. https://doi.org/10.1016/S0082-0784(89)80112-2.

[70] Cho Y, Kim YH, Kim S. Planar limit-assisted structural interpretation of saturates/aromatics/resins/asphaltenes fractionated crude oil compounds observed by Fourier transform ion cyclotron resonance mass spectrometry. Anal Chem 2011;83 (15):6068–73. https://doi.org/10.1021/ac2011685.

[71] Reilly PTA, Gieray RA, Whitten WB, Ramsey JM. Fullerene evolution in flame-generated soot. J Am Chem Soc 2000;122(47):11596–601.

[72] Santos VG, Fasciotti M, Pudenzi MA, Klitzke CF, Nascimento HL, Pereira RCL, et al. Fullerenes in asphaltenes and other carbonaceous materials: natural constituents or laser artifacts. Analyst 2016;141:2767. https://doi.org/10.1039/C5AN02333E.

[73] Pereira TMC, Vaninia G, Tose LV, Cardoso FMR, Fleming FP, Rosa PTV, et al. FT-ICR MS analysis of asphaltenes: asphaltenes go in, fullerenes come out. Fuel 2014; 131:49–58. https://doi.org/10.1016/j.fuel.2014.04.049.

[74] Labrador H, Acevedo S, Puerta L, Bouyssiere B, Carrier H. Analysis of the photo conversion of asphaltenes using laser desorption ionization mass spectrometry:

fragmentation, ring fusion, and fullerene formation. J Petrol Sci Technol 2018;8 (2):57–69.

[75] Herod AA, Stokes BJ, Hancock P, Kandiyoti R, Parker JE, Johnson CAF, et al. J Chem Soc Perkin 1994;2:499–506.

[76] Cristadoro A, Kulkarni SU, Burgess WA, Cervo EG, Räder HJ, Müllen K, et al. Structural characterization of the oligomeric constituents of petroleum pitches. Carbon 2009;47(10):2358–70.

[77] Russo C, Ciajolo A, Stanzione F, Tregrossi A, Oliano MM, Carpentieri A, et al. Investigation on chemical and structural properties of coal- and petroleum-derived pitches and implications on physico-chemical properties (solubility, softening and coking). Fuel 2019;245:478–87. https://doi.org/10.1016/j.fuel.2019.02.040.

[78] Apicella B, Ciajolo A, Suelves I, Morgan TJ, Herod AA, Kandiyoti R. Structural characterisation of products from fuel rich combustion: an approach based on size exclusion chromatography. Combust Sci Tech 2002;174(11–12):403–17. https://doi.org/10.1080/713712962.

[79] Apicella B, Millan M, Herod AA, Carpentieri A, Pucci P, Ciajolo A. Separation and measurement of flame-formed high molecular weight polycyclic aromatic hydrocarbons by size-exclusion chromatography and laser desorption/ionization time-of-flight mass spectrometry. Rapid Commun Mass Spectrom 2006;20(7): 1104–8.

[80] Onasch TB, Fortner EC, Trimborn AM, Lambe AT, Tiwari AJ, Marr LC, et al. Investigations of SP-AMS carbon ion distributions as a function of refractory black carbon particle type. Aerosol Sci Technol 2015;49(6):409–22. https://doi.org/10.1080/02786826.2015.1039959.

[81] Apicella B, Pré P, Rouzaud JN, Abrahamson J, Wal RLV, Ciajolo A, et al. Laser-induced structural modifications of differently aged soot investigated by HRTEM. Combust Flame 2019;204:13–22. https://doi.org/10.1016/j.combustflame.2019.02.026.

[82] Harris PJF. New perspectives on the structure of graphitic carbons. Crit Rev Solid State Mater Sci 2005;30(4):235–53. https://doi.org/10.1080/10408430500406265.

[83] Davis J, Molnar E, Novosselov I. Nanostructure transition of young soot aggregates to mature soot aggregates in diluted diffusion flames. Carbon 2020;159:255–65. https://doi.org/10.1016/j.carbon.2019.12.043.

[84] Kholghy M, Saffaripour M, Yip C, Thomson MJ. The evolution of soot morphology in a laminar coflow diffusion flame of a surrogate for Jet A-1. Combust Flame 2013; 160(10):2119–30. https://doi.org/10.1016/j.combustflame.2013.04.008, 0.92.

[85] Johansson KO, Head-Gordon MP, Schrader PE, Wilson KR, Michelsen HA. Resonance-stabilized hydrocarbon-radical chain reactions may explain soot inception and growth. Science 2018;361(6406):997–1000. https://doi.org/10.1126/science.aat3417.

[86] Apicella B, Tregrossi A, Oliano MM, Russo C, Ciajolo A. On-line fast analysis of light hydrocarbons, PAH and radicals by molecular-beam time of flight mass spectrometry. Chemosphere 2021;276:130174. https://doi.org/10.1016/j.chemosphere.2021.130174.

[87] Russo C, Stanzione F, Tregrossi A, Alfè M, Ciajolo A. The effect of temperature on the condensed phases formed in fuel-rich premixed benzene flames. Combust Flame 2012;159:2233. https://doi.org/10.1016/j.combustflame.2012.02.014.